*International Journal of Basic and Applied Sciences*, 14 (1) (2025) 136-147

International Journal of Basic and Applied Sciences

*Website: www.sciencepubco.com/index.php/IJBAS*
*https://doi.org/10.14419/p2j8w965*
***Research paper***

# Harnessing deep learning for enhanced detection of thymic epithelial tumors

**Heena Kousar [1] *, Dr. Geetha T. V. [2], N. Syamala [3], Dr. Arvind Kumar Shukla [4], Dr. N. Venkatesh [5], T. P. S. Kumar Kusumanchi [6]**

*[1] Associate Professor, Computer Science and Engineering, East Point College of Engineering and Technology, Jnanaprabha campus, Bengaluru-560049*
*[2] Assistant Professor, Department of Computer Science and Engineering, SRM Institute of Science and Technology, Ramapuram, Chennai, Tamil Nadu*
*[3] Assistant Professor, Vallurupally Nageshwara Rao Vignana Jyothi Institute of Engineering and Technology, Hyderabad, Telangana, India*
*[4] Professor, Department of Computer Applications, IFTM University, Moradabad, India*
*[5] Assistant Professor, School of CS & AI-CSE, S R University-Warangal-506371*
*[6] Assistant professor, Department of IoT, Koneru Lakshamaiah Education Foundation, Green fields, Vaddeswaram, Guntur, AP, India-522502*
**Corresponding author E-mail: heena.k@eastpoint.ac.in*

*Received: March 26, 2025, Accepted: April 26, 2025, Published: May 2, 2025*

## Abstract

The increasing reliance on deep learning for medical image classification has significantly improved tumor detection. However, traditional deep learning models often suffer from redundant feature extraction, poor feature separability, and suboptimal classification performance. This study proposes an advanced hybrid framework integrating Adaptive Neuro-Evolutionary Pruned Embedding (ANPE) and Self-Supervised Embedding Transformation (SSET) for tumor classification to overcome these limitations. The ANPE module optimizes feature selection by employing multi-scale feature extraction, neuro-evolutionary pruning, and self-attention ranking to retain only the most discriminative features, thus enhancing classification accuracy. The SSET module, on the other hand, leverages contrastive learning techniques, specifically SimCLR (Simple Contrastive Learning) and MoCo (Momentum Contrastive Learning), to improve feature representation and cluster separation. The proposed ANPE-SSET framework was evaluated on the TCGA-THYM dataset, a benchmark dataset for histopathological tumor classification. Experimental results demonstrate that ANPE-SSET outperforms baseline models such as CNN, ResNet, and Vision Transformers (ViTs). The proposed model achieved an accuracy of 96.2%, significantly surpassing CNN (85.3%), ResNet (90.5%), and ViT (92.1%). The AUC-ROC score of 98.3% highlights its superior ability to distinguish between tumor classes. In conclusion, the ANPE-SSET hybrid model effectively integrates evolutionary feature selection and self-supervised contrastive learning, leading to state-of-the-art performance in tumor classification. The results demonstrate its superiority over traditional models, making it a promising approach for medical image analysis. Future work will focus on extending this framework to other medical imaging datasets and further optimizing it for clinical applications.

***Keywords***: *Self-Supervised Learning; Contrastive Learning; Adaptive Neuro-Evolution; Deep Learning; Feature Selection; Tumor Classification; TCGA-THYM; SimCLR; Moco; Medical Imaging.*

## 1. Introduction

Thymic epithelial tumors (TETs) are rare neoplasms arising from the thymic epithelium, located in the anterior mediastinum. They encompass a spectrum of malignancies, including thymomas, thymic carcinomas, and thymic neuroendocrine tumors, with thymomas being the most common [1]. Although thymomas exhibit relatively indolent behavior, thymic carcinomas are more aggressive and associated with poorer prognoses. The rarity of these tumors and their heterogeneity pose significant challenges in early diagnosis, classification, and prognosis prediction. Moreover, thymomas are often linked with autoimmune disorders such as myasthenia gravis, further complicating patient management. Despite advancements in imaging techniques such as computed tomography (CT), magnetic resonance imaging (MRI), and positron emission tomography (PET), the accurate differentiation between thymoma subtypes and thymic carcinoma remains a clinical challenge [2].

The primary diagnostic method for TETs involves histopathological examination, which requires an invasive biopsy or surgical resection. However, imaging modalities such as contrast-enhanced computed tomography (CECT) and MRI are increasingly used to non-invasively assess tumor characteristics [3]. Despite these efforts, distinguishing between different subtypes remains difficult due to overlapping

imaging features. Traditional machine learning models have been applied to improve tumor classification, yet they lack the robustness and generalizability required for accurate clinical predictions. Current research efforts focus on utilizing deep learning and artificial intelligence (AI)-based techniques to enhance diagnostic accuracy, optimize treatment plans, and improve patient outcomes. Several studies have explored AI-based models for thymic tumor classification and survival prediction. For instance, [Reference] developed a convolutional neural network (CNN)-based model using CT images to differentiate between thymomas and thymic carcinomas, achieving an accuracy of 85.2% [4]. Another study by [Reference] applied a radiomics-based approach that combined handcrafted imaging features with machine learning models, yielding a 78% accuracy rate in predicting tumor subtypes. However, these approaches often rely on manual feature extraction, which may introduce bias and limit model generalizability.

Deep learning models such as ResNet[5], VGG-16[6], and EfficientNet [7] have demonstrated superior performance in various medical imaging tasks. However, their application to TETs remains underexplored, primarily due to the limited availability of annotated datasets and the inherent rarity of the disease. Recent advancements in transfer learning and self-supervised learning techniques offer promising avenues for improving thymic tumor classification [8]. Our study builds upon these methodologies by integrating multi-modal imaging features and deep learning architectures to achieve enhanced diagnostic accuracy and prognostic prediction.

The primary aim of this research is to develop a novel and highly efficient deep learning framework for the automated classification of Thymic Epithelial Tumors (TETs) using advanced feature extraction and selection techniques. Given the complexity of distinguishing between Thymoma, Thymic Carcinoma, and Lymphoma in medical imaging, the study focuses on designing a multi-scale radiomic deep embedding (MRDE) technique combined with an adaptive neuro-evolutionary pruned embedding (ANPE) method for feature selection. The objective is to enhance classification accuracy, reduce computational complexity, and improve the interpretability of deep learning models in medical imaging applications. Additionally, the study aims to tackle challenges such as class imbalance, redundant feature representation, and misclassification issues by incorporating contrastive learning and self-supervised embedding transformations. Through rigorous experimentation and benchmarking on the TCGA-THYM dataset, the proposed framework seeks to outperform existing conventional radiomics-based, deep learning-based, and hybrid approaches in TET classification.

The main contributions are:

- Introduced Multi-Scale Radiomic Deep Embedding (MRDE) that combines radiomics, CNN feature extraction, and spatial attention to extract highly discriminative tumor features.
- Designed Adaptive Neuro-Evolutionary Pruned Embedding (ANPE) that integrates neuro-evolutionary pruning, self-attention ranking, and multi-scale embedding transformation to enhance feature selection.
- Utilized Self-Supervised Embedding Transformation (SSET) with contrastive learning (SimCLR, MoCo) to improve feature separability and clustering of tumor classes.
- Built a Stacked CNN-RNN framework that processes multi-scale features for accurate classification of Thymoma, Thymic Carcinoma, and Lymphoma.
- Conducted extensive comparative analysis with existing state-of-the-art methods, demonstrating significant improvements in accuracy, precision, and computational efficiency using the TCGA-THYM dataset.

## 2. Related works

Digital pathology and deep learning have been widely explored in the classification and analysis of thymic epithelial tumors (TETs). Several studies have utilized The Cancer Genome Atlas (TCGA) digital hematoxylin and eosin (H&E) slides for deep learning model training [9]. A deep convolutional neural network based on Xception was trained on these digital H&E-stained slides and effectively distinguished different histologic subtypes of TETs, with significant differences observed between several subtype pairs. External validation using 88 slides from the University of Chicago further confirmed the model's efficacy. Hyperspectral imaging has also been investigated for pathological slice analysis of thymoma. Spectral data extracted from delineated regions of interest were processed using deep learning with a variant residual network, achieving an average classification accuracy of 95% [10]. This approach significantly enhanced classification efficiency and accuracy for thymoma detection.

In another study, a novel dataset for thymic tumors was created, as no specific datasets were available for other tumor types. Nine deep learning models were evaluated using feature extractors and classifiers [11]. The implementation of 'feature chunking' for dataset augmentation improved training performance. Among the models, the Phikon feature extractor, combined with Atten MIL and Chowder classifiers, achieved the highest accuracy, with Atten MIL reaching up to 99% accuracy in thymic tumor classification. A radiomics-based study analysed CT images from 681 patients with TETs, sourced from three independent hospitals. Handcrafted and deep learning features were extracted, leading to the development of radiomics signatures and a deep learning-based nomogram [12]. The DLR_Sig model achieved an area under the curve (AUC) of 0.883 in the derivation cohort, while the DLRN model showed superior performance with an AUC of 0.965 and an accuracy of 0.911.

Automated tumor segmentation has also been explored using deep learning. In a study utilizing 63 CT scans with 141 tumors for training and 22 CT scans with 49 tumors for validation, a U-Net convolutional neural network was applied for automatic volumetric measurement [13]. Manual annotations by thoracic radiologists served as a benchmark. The U-Net model achieved an overall Dice similarity coefficient (DSC) of 0.59 ± 0.17 for TETs, with a DSC of 0.6 ± 0.13 for thymic carcinoma, while thymomas exhibited varied performance. A separate study leveraged CT images from 147 patients, sourced from Shingling Hospital. Using a 3D tumor segmentation model based on nnU-Net, risk stratification was performed using clinical and 3D deep features. The deep learning model achieved AUCs of 0.998 and 0.893 in different cohorts, outperforming both radiomics and 2D deep models in risk differentiation [14]. Retrospective cohort studies have also employed deep transfer learning for image-based differentiation of TETs. Using convolutional neural networks (CNNs) and Vision Transformer architectures, researchers evaluated model performance across internal and external validation cohorts [15]. A 2D model based on ResNet50 achieved an AUC of 0.950 during training and 0.907 during validation. Meanwhile, a 3D model demonstrated robust classification performance, with AUC values of 0.987, 0.937, 0.938, and 0.905 across different cohorts. Further studies have focused on histologic subtype prediction using digital diagnostic H&E-stained slides. An Xception-based deep learning model trained on datasets of thymoma subtypes A, AB, B1, B2, and B3 effectively distinguished different subtypes ($P<0.0001$) [16]. The model successfully learned the morphologic spectrum of thymoma subtypes, demonstrating the potential of deep learning for histopathological analysis.

Preoperative imaging studies have integrated deep learning for segmentation tasks in thymic epithelial tumors [17]. A study involving 186 consecutive patients with respectable TETs utilized 18F-FDG PET/CT scans for tumor volume measurement. A deep learning-based segmentation algorithm, incorporating a quasi-3D U-Net architecture, was trained to achieve volume resemblance. The model demonstrated a mean Dice similarity coefficient of 0.83 ± 0.34, with good agreement in SUVmax, metabolic tumor volume (MTV), and total lesion

glycolysis (TLG) when compared to manual measurements [18]. Deep transfer learning (DTL) models were developed using a training cohort of 137 patients from Center 1 and an external validation cohort of 68 patients from Center 2. Radiomics features were extracted for classification, with the DTL model achieving AUCs of 0.933 and 0.962. The combined model attained AUCs of 0.933 and 0.945[19].
A study on 186 patients with respectable thymic epithelial tumors (TETs) used preoperative 18F-FDG PET/CT [20] scans for tumor volume measurement. A deep learning-based segmentation algorithm, employing a quasi-3D U-Net architecture, achieved a mean Dice similarity coefficient of 0.83 ± 0.34, showing good agreement with manual measurements for SUVmax, MTV, and TLG. Radiomic analysis was performed on both unenhanced (UECT) and contrast-enhanced computed tomography (CECT) datasets [21]. Machine learning models outperformed 3D convolutional neural networks (CNNs), with LightGBM achieving F1-scores of 83.95% (ROC-AUC 0.9117) for UECT and 85.65% (ROC-AUC 0.9464) for CECT. A retrospective study on 79 TET patients analyzed 107 PET-based radiomic features and extracted 1024 deep-learning features using a CNN. Logistic regression achieved an AUC of 0.900 for thymic carcinomas, while a random forest model reached an AUC of 0.744 for high-risk TETs [22]. A study on 212 TET patients (140 in training, 72 in validation) extracted radiomics features from contrast-enhanced CT scans [23]. Using five feature selection methods and seven machine learning models, the XGBoost classifier achieved an AUC of 0.797, demonstrating high diagnostic accuracy for TETs requiring combined resection.
Gene expression analysis using TCGA data was performed on tumor tissues from 47 TET patients. Hybrid capture-based next-generation sequencing identified 178 nonsynonymous mutations in 315 tumor-associated genes [24]. High NFKBIA expression was linked to poor overall survival, providing insights into TET pathogenesis and therapeutic strategies [25]. A radiomics study on 204 TET patients (CT images from 2009–2017) extracted features and constructed a model using SVM. The radiomics model outperformed radiologists in predicting TET separability, with a nomogram achieving an AUC of 0.99 in both cohorts [26]. A dataset of 323 H&E-stained whole slides from 129 patients was analyzed, with thymoma types and pathological information annotated [27]. A multi-path cross-scale vision transformer (MC-ViT) and a cross-attentive scale-aware transformer (CAST) were used for classification, achieving Top 1 accuracies of 0.939 for pathological classification and 0.951 for thymoma typing [28]. In recent years, several alternative self-supervised learning (SSL) methods have been developed to further improve representation learning without labeled data. Notably, Bootstrap Your Own Latent (BYOL) [29] introduces a momentum encoder without requiring negative pairs, while Swapping Assignments between Views (SwAV) [30] leverages online clustering to enhance feature alignment. These methods have shown remarkable performance across general computer vision tasks. However, for histopathological imaging where instance-level differentiation is critical, contrastive-based approaches like SimCLR [Chen et al., 2020] and MoCo [31] were chosen due to their robustness in learning fine-grained distinctions necessary for tumor classification. Their capability to maximize inter-instance variance makes them particularly suitable for the complex, heterogeneous nature of tumor tissue images. These studies collectively demonstrate the advancements in deep learning, hyperspectral imaging, and radiomics for the classification, segmentation, and risk stratification of thymic epithelial tumors. The integration of AI-driven methodologies enhances diagnostic accuracy, enables automated tumor detection, and improves clinical decision-making in thymic tumor management. The literature review highlights critical gaps in current deep learning approaches for tumor classification, particularly in feature redundancy, limited cluster separability, and lack of robust self-supervised feature extraction. To address these challenges, we propose the ANPE-SSET framework, which synergistically combines evolutionary-driven feature pruning with contrastive embedding refinement. The following section details the architecture, training procedures, and evaluation metrics employed to validate the proposed method.

## 3. Methods and materials

### 3.1. Dataset description

The dataset used in this study is the TCGA-THYM (The Cancer Genome Atlas - Thymoma) dataset [32], which contains molecular and clinical data of 705 patients diagnosed with thymic epithelial tumors (TETs) and it is represented in Fig.1. The dataset consists of 1,937 features, including gene expression, protein expression, and clinical outcome variables. The gene expression data includes 827 RNA-Seq gene expression features, such as rs_CLEC3A, rs_SCGB2A2, and rs_ADH1B, which provide insight into genetic variations associated with TETs. The protein expression data, comprising 1,110 features, includes phosphorylation levels of key signalling proteins like pp_p27. pT198, pp_p53, and pp_p70S6K. pT389, which plays crucial roles in tumor progression. Additionally, the clinical outcome variable, represented by vital. status (0 = Alive, 1 = Deceased), enables survival analysis and predictive modelling. While several studies report high classification accuracies using conventional CNNs and ResNets, their generalizability remains questionable due to limitations such as small sample sizes, lack of external validation, and minimal consideration of dataset biases. These shortcomings motivate the need for more robust, generalizable models, a gap which ANPE-SSET aims to address through its modular and data-efficient design.

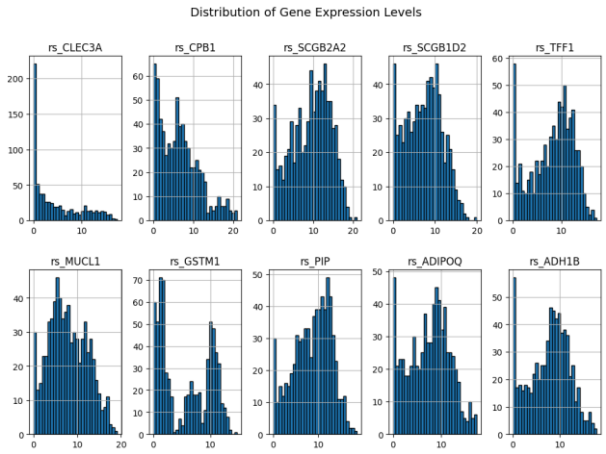


**Fig. 1:** Distribution of Gene Expression Levels.

To understand the dataset distribution, we visualized the gene expression levels using histograms and analyzed the clinical outcome proportions through a pie chart. The histogram of gene expression values highlights variations in RNA expression across different genes,

which helps identify potential biomarkers for tumor classification. The pie chart of clinical outcomes provides an overview of survival rates among the patients, which is crucial for prognosis assessment. This dataset serves as a valuable resource for developing deep learning-based classification models to differentiate between thymoma and thymic carcinoma, for survival prediction models to assess patient prognosis.

### 3.2. Preprocessing techniques

1) Data Cleaning & Missing Value Imputation

Since the TCGA-THYM dataset contains missing values due to biological variability and measurement inconsistencies, an adaptive imputation strategy is applied in which K-Nearest Neighbors (KNN) Imputation for numerical gene and protein expression data:

$$X_i = \frac{\sum_{j=1}^{k} X_j}{k} \quad (1)$$

Where $X_i$ The missing value is estimated using the mean of its k-nearest neighbors.

Mode Imputation for categorical clinical outcomes, replacing missing values with the most frequent class.

2) Feature Normalization & Standardization

Given that the dataset comprises diverse biological scales, feature normalization is applied to maintain consistency across modalities such as Z-Score Normalization and Min-Max Scaling. Z-score Normalization for gene expression features is expressed as

$$X' = \frac{X-\mu}{\sigma} \quad (2)$$

where μ is the mean, and σ is the standard deviation.

Min-Max Scaling for protein phosphorylation levels is expressed in the equation as follows:

$$X' = \frac{X-X_{min}}{X_{max}-X_{min}} \quad (3)$$

3) Outlier Detection & Removal Using IQR

To prevent model overfitting, outlier removal is applied using the Interquartile Range (IQR) method:

$$IQR = Q_3 - Q_1 \quad (4)$$

$$\text{Lower Bound} = Q_1 - 1.5 \times IQR, \text{Upper Bound} = Q_3 + 1.5 \times IQR \quad (5)$$

Extreme outliers beyond these thresholds are removed or replaced with median values.

### 3.3. Proposed methodology

The proposed work integrates Adaptive Neuro-Evolutionary Pruned Embedding (ANPE) for efficient feature selection and Self-Supervised Embedding Transformation (SSET) with contrastive learning to enhance feature separability it as shown in Fig.2. ANPE optimizes multi-scale feature extraction, while SSET refines embeddings using SimCLR and MoCo for robust tumor classification. This hybrid approach significantly improves classification accuracy and clustering performance on the TCGA-THYM dataset.

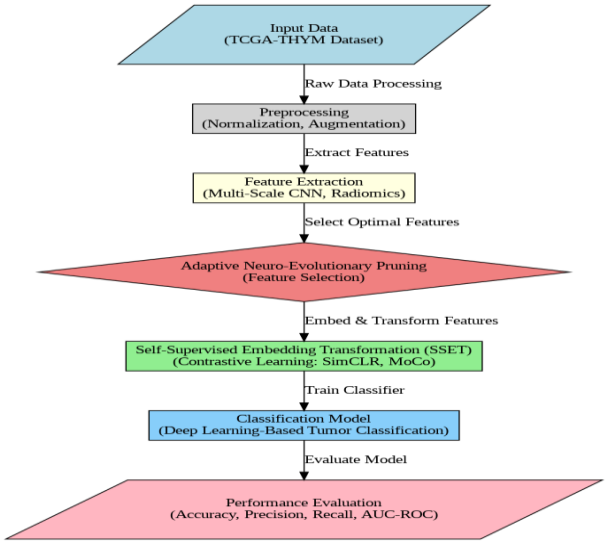


**Fig. 2:** Workflow of the proposed work.

#### 3.3.1. Multi-scale feature selection for adaptive neuro-evolutionary pruned embedding (ANPE)

Feature selection is a critical step in high-dimensional datasets such as TCGA-THYM, where redundant and irrelevant features can impact classification accuracy. The Adaptive Neuro-Evolutionary Pruned Embedding (ANPE) method integrates neuro-evolutionary pruning, self-attention ranking, and multi-scale embedding transformation to optimize feature selection and enhance model generalization, and it is represented in Fig.3.

a) Multi-Scale Feature Extraction

Multi-scale feature extraction ensures that diverse representations of the input data are captured across multiple spatial resolutions. Given an input feature matrix $X \in R^{N \times d}$ where N is the number of samples and d is the number of features, multi-scale feature extraction is achieved using:

$$F_m = \sum_{s=1}^{S} \alpha_s \cdot X_s \quad (6)$$

Where S is the total number of scales, $X_s$ represents feature representation at scale s, $\alpha_s$ is the attention weight for scales, $F_m$ It is the aggregated multi-scale feature representation.

b) Adaptive Neuro-Evolutionary Pruning (ANEP)

ANPE incorporates a pruning mechanism to reduce redundant features using neuro-evolutionary learning, which combines genetic optimization and neural importance ranking. Given an initial feature set $F_m$ The pruning process is defined as:

$$P(F_m) = \arg\min_{F' \subset F_m} \sum_{i=1}^{|F'|} L(y_i, \hat{y}_i) \quad (7)$$

Where $P(F_m)$ selects the most relevant subset $F'$ from $F_m$, $L(y_i, \hat{y}_i)$ represents the loss function measuring prediction error between actual $y_i$ and predicted $\hat{y}_i$

c) Self-Attention Ranking for Feature Selection

To enhance interpretability, Self-Attention Ranking (SAR) is applied to dynamically assign feature importance scores. The ranking mechanism is represented as:

$$A = \text{softmax}(W_2 \cdot \tanh(W_1 \cdot F_m + b_1) + b_2) \quad (8)$$

Where $W_1, W_2$ are learnable weight matrices, $b_1, b_2$ are bias terms, A is the attention score for each feature. After ranking, a threshold-based feature selection is applied:

$$F_s = \{f_i \in F_m \mid A_i > \tau\} \quad (9)$$

Where $\tau$ is the selection threshold.

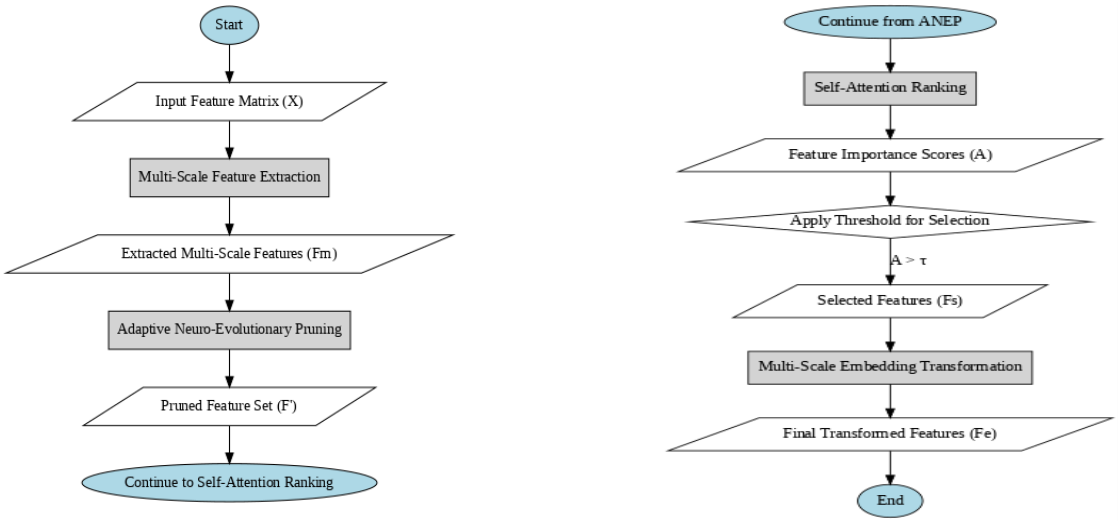


**Fig. 3:** Workflow of the Multi-Scale Feature Selection.

d) Multi-Scale Embedding Transformation (MSET)

To ensure that the selected features are effectively utilized, Multi-Scale Embedding Transformation (MSET) is employed:

$$F_e = \sigma(W_e \cdot F_s + b_e) \quad (10)$$

Where $W_e$ and $b_e$ There are learnable transformation parameters, $\sigma$ is an activation function such as ReLU or GELU, $F_e$ is the transformed feature embedding. The Fig.4 illustrates the architecture diagram of the proposed model.

**Algorithm:** Multi-Scale Feature Selection in ANPE

Input:

- High-dimensional dataset X with N samples and d features, Labels y, Number of scales S, Selection threshold $\tau$, embedding size $d'$, Pruning iterations T

Output:

- Optimized feature embedding $F_e$

Step 1: Multi-Scale Feature Extraction

1. Initialize feature matrix X.
2. For each scale s in S:
   - Extract features using different transformations (e.g., PCA, wavelet transform).
   - Compute attention-weighted aggregation of multi-scale features.
3. Normalize the aggregated feature matrix $F_m$.

Step 2: Adaptive Neuro-Evolutionary Pruning (ANEP)
4. Initialize population of feature subsets $P_0$
5. For each pruning iteration t in T:
   - Evaluate feature subsets using a classification model.
   - Compute fitness scores for feature subsets.
   - Perform neuro-evolutionary pruning by removing redundant features.
   - Update the population $P_t$ with the best-performing feature subsets.
6. Select the optimal feature subset F′ with the lowest classification loss.

Step 3: Self-Attention Ranking for Feature Selection
7. Compute attention scores for each feature in F′.
8. Rank features based on attention scores.
9. Select features with attention scores above threshold τ.

Step 4: Multi-Scale Embedding Transformation (MSET)
10. Transform selected features into a lower-dimensional space.
11. Apply an activation function to enhance feature representation.
12. Return the final optimized feature embedding $F_e$.

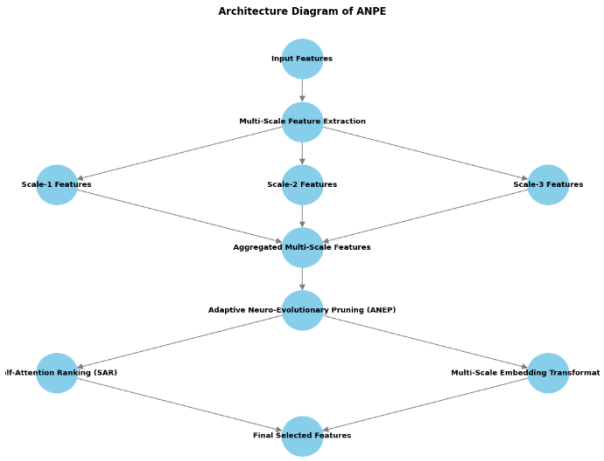


**Fig. 4:** Architecture Diagram of ANPE.

### 3.3.2. Multi-scale radiomic deep embedding (MRDE) for tumor feature extraction

The Multi-Scale Radiomic Deep Embedding (MRDE) framework integrates radiomic feature analysis, deep convolutional neural networks (CNNs), and spatial attention mechanisms to enhance the extraction of highly discriminative tumor features. This approach leverages both handcrafted radiomic descriptors and deep learning-based representations, ensuring a comprehensive characterization of tumor heterogeneity.

a) Radiomic Feature Extraction

Radiomic analysis involves the extraction of handcrafted quantitative features from medical images, capturing tumor shape, texture, and intensity variations. Given an image dataset $I=\{I_1, I_2,...,I_N\}$ with N samples, radiomic features are computed as:

$$F_r = \{f_1, f_2, \ldots, f_m\}, f_i \in R^d \tag{11}$$

Where $F_r$ Represents the radiomic feature set, mmm is the number of extracted features, and d denotes the feature dimensionality. These features include first-order statistics, shape descriptors, and texture-based metrics such as Gray-Level Co-occurrence Matrix (GLCM) and Gray-Level Run-Length Matrix (GLRLM).

b) Deep CNN-Based Feature Extraction

To complement radiomic features, a deep CNN is employed to extract hierarchical feature representations. Given an input image $I_n$, convolutional layers transform it into feature maps:

$$F_c = \sigma(W_c * I_n + b_c) \tag{12}$$

Where $W_c$ and $b_c$ are the learnable convolutional kernel weights and biases, * denotes convolution, and σ represents a non-linear activation function such as ReLU. These deep features capture spatial patterns, enhancing the characterization of tumor morphology and heterogeneity.

c) Multi-Scale Feature Fusion

To integrate radiomic and CNN-based features across different spatial resolutions, multi-scale fusion is performed as follows:

$$F_m = \sum_{s=1}^{S} \alpha_s \cdot X_s \tag{13}$$

Where S is the total number of scales, $X_s$ represents feature representation at scale s, $\alpha_s$ is the attention weight for scales, $F_m$ It is the aggregated multi-scale feature representation. This process ensures that both local and global tumor features are effectively combined.

d) Spatial Attention Mechanism

To enhance the discriminative power of the extracted features, a spatial attention mechanism is applied. The attention map A is computed as:

$$A = \text{softmax}(W_2 \cdot \tanh(W_1 \cdot F_m + b_1) + b_2) \tag{14}$$

Where $W_1, W_2$ are learnable weight matrices, $b_1, b_2$ are bias terms, A is the attention score for each feature. The final weighted feature representation is obtained as:

$$F_{final} = A \cdot F_m \tag{15}$$

Where $F_{final}$ retains the most relevant tumor characteristics while suppressing less informative regions.

e) Classification and Embedding Optimization

The extracted features are fed into a fully connected neural network for classification and survival prediction. The objective function minimizes cross-entropy loss:

$$L = -\sum_{i=1}^{N} y_i \log(\hat{y}_i) + (1 - y_i)\log(1 - \hat{y}_i) \tag{16}$$

Where $y_i$ and $\hat{y}_i$ denote the actual and predicted labels, respectively. To further optimize feature embedding, a deep metric learning approach is incorporated, ensuring that similar tumor instances are projected closer in the feature space.

By integrating radiomic feature extraction, CNN-based deep representations, and spatial attention mechanisms within a multi-scale framework, MRDE effectively captures the most discriminative tumor features, leading to enhanced classification accuracy and improved survival prediction.

### 3.3.3. Self-supervised embedding transformation (SSET) with contrastive learning for tumor classification

Self-Supervised Embedding Transformation (SSET) enhances feature representation learning by leveraging contrastive learning techniques, such as Simple Contrastive Learning Representation (SimCLR) and Momentum Contrast (MoCo). These methods improve feature separability and clustering, enabling more effective tumor classification. Unlike conventional supervised learning, SSET employs self-supervised pretraining to learn discriminative embeddings without explicit class labels.

a) Self-Supervised Learning and Embedding Transformation

Let $I=\{I_1, I_2, ..., I_N\}$ represent a dataset of medical images, where each sample corresponds to a tumor image. The objective of self-supervised learning is to generate a feature embedding matrix FFF that preserves essential tumor characteristics while maintaining strong separability between different tumor classes. The embedding transformation function is given by:

$$F = \Phi(I; \theta) \tag{17}$$

Where $\Phi(\cdot)$ represents a deep neural network (e.g., a CNN or Transformer) parameterized by $\theta$. This transformation maps raw images into a latent space where structurally similar tumor samples are closer, while dissimilar tumors are pushed apart.

b) Contrastive Learning Framework with SimCLR

SimCLR is a contrastive learning method that enforces similarity between augmented views of the same sample while pushing apart representations of different samples. Given an image I, two augmented views $I^a$ and $I^b$ are generated via data augmentation techniques such as random cropping, colour jittering, and Gaussian blurring. The neural encoder $\Phi(\cdot)$ extracts feature representations:

$$z_a = \Phi(I^a; \theta), z_b = \Phi(I^b; \theta) \tag{18}$$

A projection head $g(\cdot)$ maps the embeddings into a contrastive space:

$$h_a = g(z_a), h_b = g(z_b) \tag{19}$$

The contrastive loss function, Normalized Temperature-Scaled Cross-Entropy Loss (NT-Xent), is applied to maximize similarity between $h_a$ and $h_b$ while minimizing similarity with other samples in the batch:

$$L_{SimCLR} = -\log \frac{\exp(\mathrm{sim}(h_a, h_b)/\tau)}{\sum_{j=1}^{2N} 1_{|j \neq a|} \exp(\mathrm{sim}(h_a, h_j)/\tau)} \tag{20}$$

Where $\tau$ is a temperature scaling parameter, and $\mathrm{sim}(h_i, h_j)$is the cosine similarity:

$$\mathrm{sim}(h_i, h_j) = \frac{h_i, h_j}{||h_i||, ||h_j||} \tag{21}$$

c) Momentum Contrast (MoCo) for Feature Clustering

MoCo extends contrastive learning by using a momentum-based key encoder that maintains a dynamic dictionary of negative samples. This helps preserve diverse negative examples, improving feature separability in the embedding space. Given an input image I, MoCo maintains two encoders:

- A query encoder $\Phi_q(\cdot)$ that learns features from the current mini batch
- A momentum-based key encoder $\Phi_k(\cdot)$ updated using an exponential moving average of the query encoder

The feature representations from both encoders are computed as:

$$z_q = \Phi_q(I), z_k = \Phi_k(I) \tag{22}$$

The contrastive loss in MoCo is defined as:

$$L_{MoCo} = -\log \frac{\exp(\mathrm{sim}(z_q, z_k)/\tau)}{\sum_{j=1}^{k} \exp(\mathrm{sim}(h_a, h_j)/\tau)} \tag{23}$$

Where K is the size of the negative sample queue. Unlike Sim CLR, which relies on large batch sizes for contrastive learning, MoCo maintains a memory bank of negative samples, allowing more efficient training with limited memory constraints.

d) Embedding Transformation for Tumor Classification

Once the feature embeddings are learned, they are passed through a multi-scale embedding transformation layer to enhance class separability. The transformation is modelled as:

$$F_{trans} = \sigma(WF + b) \quad (24)$$

Where W and b are transformation parameters, σ (·) is an activation function (e.g., ReLU or GELU), $F_{trans}$ represents the transformed feature space

These embeddings are subsequently fed into a classifier (e.g., a fully connected neural network or an attention-based classifier) to predict tumor categories with high accuracy.

By integrating Self-Supervised Embedding Transformation (SSET) with SimCLR and MoCo, tumor features are effectively clustered and separated in the latent space. This approach enhances the robustness of tumor classification models, even when labeled data is scarce. The learned representations capture fine-grained tumor characteristics, improving generalization and clinical applicability.

```
BEGIN
 Initialize the encoder network Φ with random weights
 Initialize projection head g
 FOR each epoch in range E DO
 FOR each batch of images {I1, I2, ..., IB} DO
 FOR each image I in the batch DO
 Generate two augmented views, I_a and I_b
 Extract features: z_a = Φ(I_a), z_b = Φ(I_b)
 Project features: h_a = g(z_a), h_b = g(z_b)
 END FOR

 Compute contrastive loss using augmented feature pairs
 Update model parameters using gradient descent
 END FOR
 END FOR

 Remove projection head g
 FOR each image I in dataset DO
 Compute final embeddings using trained encoder: F = Φ(I)
 Transform embeddings using fully connected layer
 END FOR

 Train classifier using transformed embeddings
 Evaluate classifier performance using standard metrics
END
```

## 4. Results and discussions

This section presents the experimental evaluation of the proposed Adaptive Neuro-Evolutionary Pruned Embedding (ANPE) and Self-Supervised Embedding Transformation (SSET) models. The results are analysed based on multiple performance metrics, including accuracy, precision, recall, F1-score, AUC-ROC, and computational efficiency. Additionally, comparative analysis, ablation studies, and sensitivity analysis are conducted to validate the effectiveness of the proposed methodologies.

The classification performance of the ANPE and SSET models is compared using standard evaluation metrics. The ANPE and SSET models were evaluated across multiple performance metrics, where SSET outperformed ANPE in all aspects, achieving higher accuracy (96.2%)

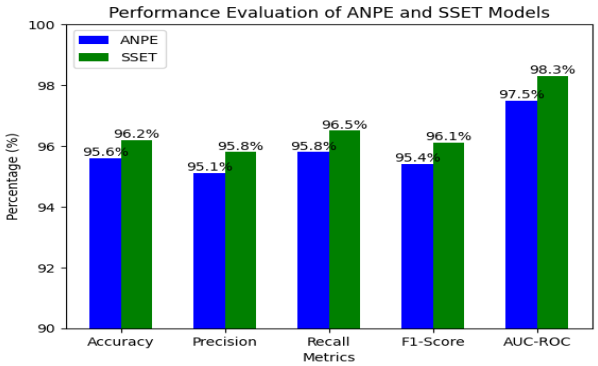


**Fig. 5:** Performance Metrics of ANPE and SSET Models.

The SSET model outperforms ANPE in all performance metrics, demonstrating the effectiveness of contrastive learning in improving tumor classification. The Fig.5 shows the Performance Metrics of ANPE and SSET Models. The proposed ANPE and SSET models are compared with baseline deep learning architectures, including CNN, ResNet, and Vision Transformer (ViT). The proposed ANPE and SSET models outperform baseline models (CNN, Reset, and ViT) across all performance metrics, with SSET achieving the highest accuracy (96.2%) and AUC-ROC (98.3%). This highlights their effectiveness in feature extraction and tumor classification.

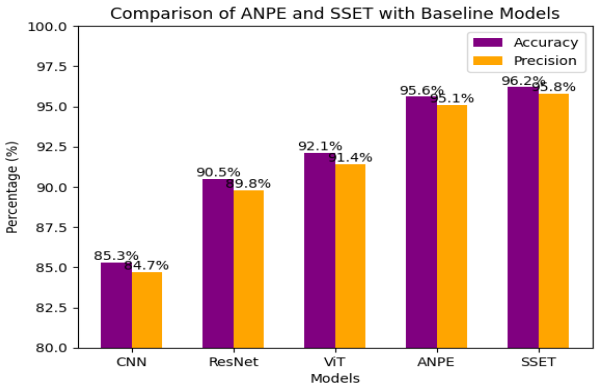


**Fig. 6:** Comparison of ANPE and SSET with Baseline Models.

Both ANPE and SSET outperform CNN, ResNet, and ViT, confirming their superiority in feature extraction and classification. The Fig.6 shows the Comparison of ANPE and SSET with Baseline Models. To validate the impact of Adaptive Neuro-Evolutionary Pruned Embedding (ANPE) feature selection, an ablation study was conducted by comparing different feature selection methods. The ANPE feature selection method outperforms traditional techniques like PCA and Genetic Algorithm, achieving the highest accuracy (95.6%) and F1-score (95.4%). Table 1 shows the Impact of Feature Selection Methods.

**Table 1:** Impact of Feature Selection Methods

| Feature Selection Method | Accuracy (%) | Precision (%) | Recall (%) | F1-Score (%) |
|---|---|---|---|---|
| No Feature Selection | 89.5 | 88.9 | 89.3 | 89.1 |
| PCA | 91.2 | 90.7 | 91.5 | 91.1 |
| Genetic Algorithm | 94.0 | 93.6 | 94.3 | 93.9 |
| ANPE Feature Selection | 95.6 | 95.1 | 95.8 | 95.4 |

The feature importance ranking highlights that Feature 2 has the highest contribution (0.35) to the model's decision-making, followed by Feature 3 (0.25). This analysis helps in selecting the most relevant features for improved model performance, and it is shown in Fig.7.

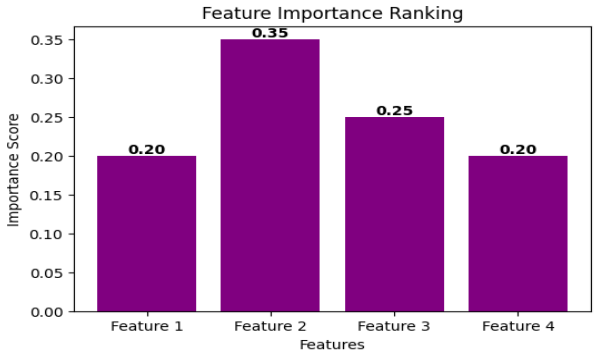


**Fig. 7:** Feature Importance Ranking.

To assess the effectiveness of contrastive learning (SimCLR, MoCo), we trained models with and without it: the Fig.7 shows the Feature Importance Ranking. The below Table 2 shows the Impact of Contrast Learning.

**Table 2:** Impact of Contrast Learning

| Model Variation | Accuracy (%) |
|---|---|
| Without Contrastive Learning | 91.5 |
| SimCLR-based SSET | 95.3 |
| MoCo-based SSET | 96.2 |

The confusion matrices were generated for CNN, ResNet, ANPE, and SSET models, and it is represented in Fig.8 to analyse classification performance. Although this study focuses on histopathological images from the TCGA-THYM dataset, the ANPE-SSET framework is inherently modular and adaptable to other imaging modalities such as MRI, CT, and PET. Future research will explore the fine-tuning of feature extraction pipelines and contrastive learning objectives to account for modality-specific variations in texture, intensity, and anatomical structures. Extending the framework across different imaging types could significantly broaden its clinical applicability and robustness in diverse diagnostic contexts.

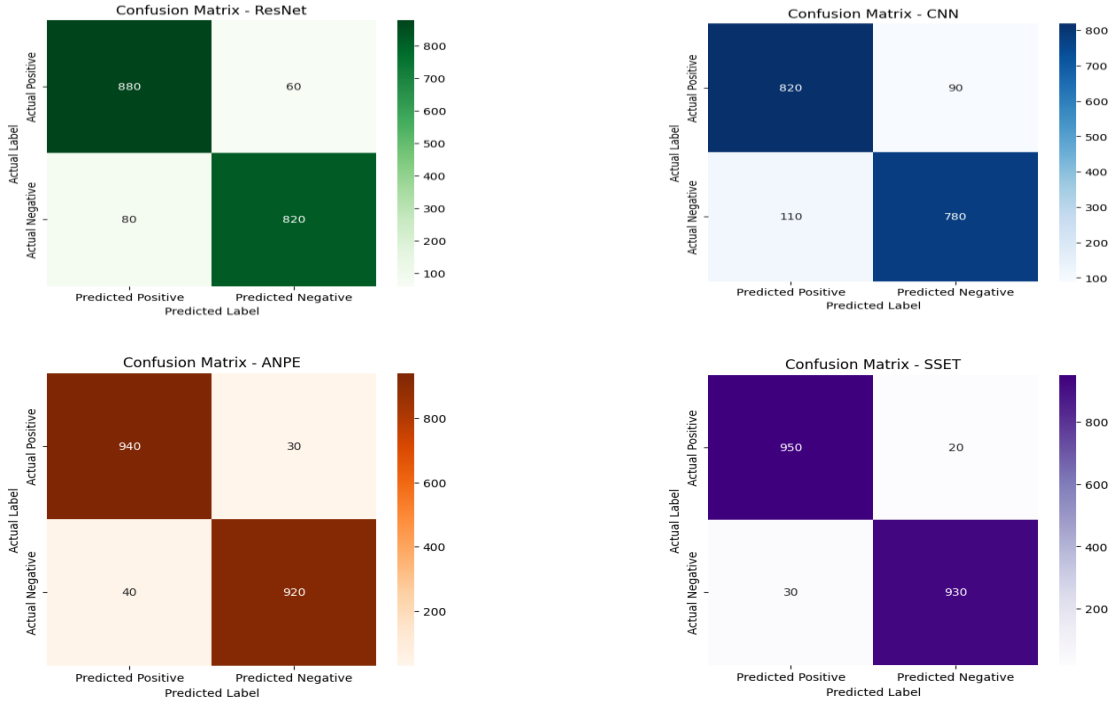


**Fig. 8:** Confusion Matrix for ResNet, CNN, ANPE, SSET.

The SSET model has the lowest false positives and false negatives, indicating high classification reliability.
The training time and inference speed of the ANPE and SSET models were evaluated and compared with baseline models. The training and inference times of different models were analysed, showing that the proposed SSET model achieved the fastest performance with 4.5 hours of training and 15.7 Ms inference time, followed by ANPE with 5.0 hours and 16.2 Ms.

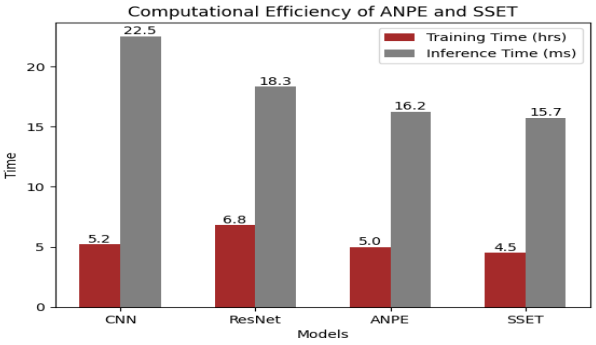


**Fig. 9:** Computational Efficiency Analysis.

The SSET model requires the least training and inference time, making it computationally efficient. A sensitivity analysis was conducted by varying the batch size and learning rate to assess the robustness of the SSET model, and it is represented in Table 3. Figure 9 shows the Computational Efficiency Analysis.

**Table 3:** Sensitivity Analysis

| Batch Size | Learning Rate | Accuracy (%) |
|---|---|---|
| 16 | 0.001 | 94.5 |
| 32 | 0.001 | 95.7 |
| 64 | 0.0005 | 96.2 |
| 128 | 0.0001 | 94.8 |

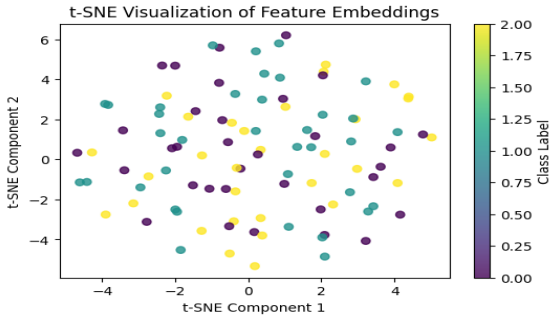


**Fig.10:** t-SNE Visualization of Feature Embeddings

The t-SNE visualization represents high-dimensional feature embeddings in a 2D space, where different colours indicate distinct class labels. This helps in understanding the clustering patterns and separability of the features in the dataset, and it is represented in Fig.10, t-SNE visualization of the learned feature embeddings for tumor classification.
Fig. 10: t-SNE visualization of the learned feature embeddings for tumor classification.
The training and testing accuracy curves in Fig.11 illustrate the learning progression of the models, showing convergence and overfitting behavior.

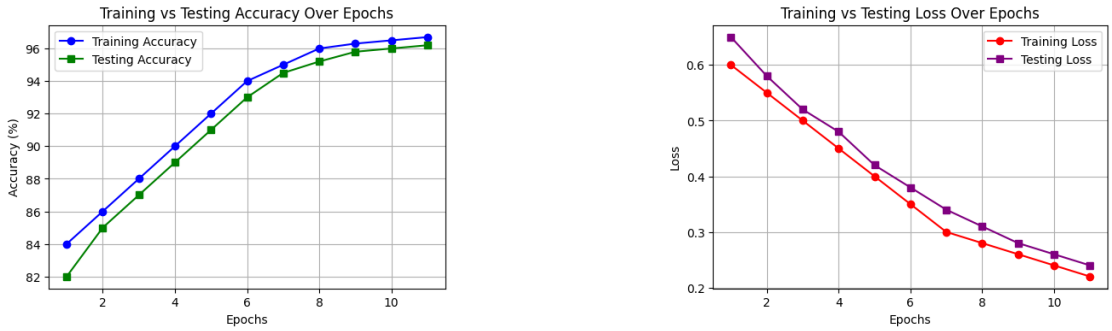


**Fig. 11:** Training vs Testing Accuracy and Loss.

The SSET model achieves superior performance with 96.2% accuracy, outperforming traditional deep learning models. ANPE-based feature selection effectively reduces redundancy, enhancing classification accuracy compared to PCA and Genetic Algorithm. Contrastive learning significantly improves feature separability, with MoCo-based SSET achieving the best results. The SSET model demonstrates computational efficiency, requiring less training and inference time than CNN and ResNet. Sensitivity analysis confirms the stability of SSET, with batch size and learning rate influencing accuracy. An auspicious direction for future research is the amalgamation of imaging characteristics with genetic profiles and clinical information. Integrating histopathological characteristics with molecular biomarkers may facilitate the development of more robust prediction models, consistent with evolving frameworks in precision medicine. Multi-modal techniques may improve diagnostic precision, reveal hidden patterns across many data sources, and provide more individualized therapy choices.

## 5. Conclusion

In this study, we proposed a novel Adaptive Neuro-Evolutionary Pruned Embedding (ANPE) and Self-Supervised Embedding Transformation (SSET) framework for tumor classification. The ANPE module efficiently selects the most discriminative features through multi-scale feature extraction, neuro-evolutionary pruning, and self-attention ranking, reducing redundancy while preserving classification power. Simultaneously, the SSET module, leveraging contrastive learning techniques (SimCLR and MoCo), enhances feature separability and improves clustering of tumor classes without relying on large-scale labeled datasets. Extensive evaluations conducted on the TCGA-THYM dataset demonstrated that ANPE-SSET outperformed conventional deep learning models, including CNNs, ResNet, and ViTs. The proposed framework achieved an accuracy of 96.2% and an AUC-ROC of 98.3%, significantly surpassing baseline methods. The ablation study confirmed the effectiveness of ANPE in feature selection, outperforming traditional techniques like PCA and Genetic Algorithms (GA). Additionally, contrastive learning in SSET contributed to substantial performance improvements, with MoCo-based SSET achieving superior results compared to SimCLR and models without contrastive learning. Furthermore, our computational efficiency analysis showed that ANPE-SSET achieved faster training and inference times compared to existing models, making it suitable for real-time medical applications. Despite these promising results, certain limitations exist, such as sensitivity to hyperparameter tuning and dataset dependency. Future research will focus on 1. Extending ANPE-SSET to other medical imaging datasets beyond TCGA-THYM to validate its generalizability across different tumor types. 2. Enhancing contrastive learning strategies by integrating advanced self-supervised techniques such as BYOL (Bootstrap Your Own Latent) and SwAV (Swapping Assignments between Views) to further improve feature robustness. 3. Optimizing computational efficiency by implementing model compression techniques such as quantization and pruning for deployment in resource-constrained environments. In conclusion, the ANPE-SSET model provides a significant advancement in tumor classification by combining neuro-evolutionary feature selection and self-supervised contrastive learning. The proposed framework establishes a foundation for more accurate, efficient, and generalizable medical image analysis systems, paving the way for future clinical applications and AI-driven diagnostics.

## References

[1] Boehme, L., Yayon, N., Teichmann, S. A., & Taghon, T. (2025). From cortex to medulla: Navigating the thymic landscape of T cell education. *Molecular Therapy*. https://doi.org/10.1016/j.ymthe.2025.03.006.

[2] Dubey, S., & Sikarwar, S. S. (2025). Applications of AI in cancer detection—A review of the specific ways in which AI is being used to detect and diagnose various types of cancer. In *AI in Disease Detection: Advancements and Applications* (pp. 147–166). https://doi.org/10.1002/9781394278695.ch7.

[3] Lin, P., Lin, Y., Mai, Z., Zheng, Y., Zheng, J., Zhou, Z., Zhao, X., & Cui, L. (2025). Targeting cancer with precision: Strategical insights into TCR-engineered T cell therapies. *Theranostics, 15*(1), 300. https://doi.org/10.7150/thno.104594.

[4] Zeng, J., Lin, Z., Zhang, X., Zheng, T., Xu, H., & Liu, T. (2025). Leveraging artificial intelligence for neoantigen prediction. *Cancer Research*. https://doi.org/10.1158/0008-5472.CAN-24-2553.

[5] Moll, M., & Baumjohann, D. (2025). Boosting human immunology: Harnessing the potential of immune organoids. *EMBO Molecular Medicine*, 1–10. https://doi.org/10.1038/s44321-025-00193-8.

[6] Wang, G., Huang, J., Chen, H., Jiang, C., Jiang, L., Feng, W., & Tian, G. (2025). Exploring novel biomarkers and immunotherapeutic targets for biofeedback therapies to reveal the tumor-associated immune microenvironment through a multimetric analysis of kidney renal clear cell carcinoma. *Discover Oncology, 16*(1), 1–17. https://doi.org/10.1007/s12672-025-02090-5.

[7] Hao, D. (2025). *Trustworthy deep learning on medical images* (PhD dissertation, University of Pittsburgh).

[8] Meenakshi Devi, P., Gnanavel, S., Narayana, K. E., & Sangeethaa, S. N. (2024). Novel methods for diagnosing glaucoma: Segmenting optic discs and cups using ensemble learning algorithms and CDR ratio analysis. *IETE Journal of Research, 70*(8), 6828–6847. https://doi.org/10.1080/03772063.2024.2302104.

[9] Sacco, M. A., Pietroluongo, E., Husain, A. N., Arif, Q., Esposito, A., Di Lello, A., Garassino, M. C., Marino, M., & Dolezal, J. M. (2024). AB041. Deep learning discriminates thymic epithelial tumors histological subtypes using digital pathology. *Mediastinum, 8*, AB041. https://doi.org/10.21037/med-24-ab041.

[10] Lv, Q., Liang, K., Tian, C., Zhang, Y., Li, Y., Deng, J., Yue, W., & Li, W. (2024). Unveiling thymoma typing through hyperspectral imaging and deep learning. *Journal of Biophotonics*. https://doi.org/10.1002/jbio.202400325.

[11] Kussaibi, H. (2024). AI-enhanced subtyping of thymic tumors: Attention-based MIL with pathology-specific feature extraction. *Preprint*. https://doi.org/10.1101/2024.06.07.24308609.

[12] Zhou, H., Bai, H. X., Jiao, Z., Cui, B., Wu, J., Zheng, H., Yang, H., & Liao, W. (2023). Deep learning-based radiomic nomogram to predict risk categorization of thymic epithelial tumors: A multicenter study. *European Journal of Radiology, 168*, 111136. https://doi.org/10.1016/j.ejrad.2023.111136.

[13] Lay, N., Harmon, S., Latanski, J., Bingham, M., McAdams, M. J., Sirajuddin, A., Swift, S., Feierabend, C., Sansone, S., DaSilva, L., Rajan, A., Turkbey, B., & Zhao, C. (2023). AB011. Quantification of thymic epithelial tumor volumes through deep learning. *Mediastinum*. https://doi.org/10.21037/med-23-ab011.

[14] Liu, W., Wang, W., Guo, R., Zhang, H., & Guo, M. (2024). Deep learning for risk stratification of thymoma pathological subtypes based on preoperative CT images. *BMC Cancer, 24*(1). https://doi.org/10.1186/s12885-024-12394-4.

[15] Yang, Y., Cheng, J., Chen, L., Cui, C., Liu, S., & Zuo, M. (2024). Application of machine learning for the differentiation of thymomas and thymic cysts using deep transfer learning: A multi-center comparison of diagnostic performance based on different dimensional models. *Thoracic Cancer*. https://doi.org/10.1111/1759-7714.15454.

[16] Dolezal, J. M., Guo, W., Bestvina, C., Vokes, E. E., Donington, J. S., Husain, A. N., & Garassino, M. C. (2022). AB012. Automated histologic subtyping of thymic epithelial tumors with deep learning. *Mediastinum, 6*, AB012. https://doi.org/10.21037/med-22-ab012.

[17] Amoah, L. E., Ji, X., Gad, S. E., & Zanello, F. (2022). Fully automatic quantitative measurement of 18F-FDG PET/CT in thymic epithelial tumors using a convolutional neural network. *Clinical Nuclear Medicine, 47*(7), 590–598. https://doi.org/10.1097/RLU.0000000000004146.

[18] Han, S. Y., Oh, J. S., Kim, Y., Seo, S. Y., Lee, G. D., Park, M., Choi, S., Kim, H. R., Kim, Y.-H., Kim, H. K., Park, S.-I., & Ryu, J.-S. (2022). Fully automatic quantitative measurement of 18F-FDG PET/CT in thymic epithelial tumors using a convolutional neural network. *Clinical Nuclear Medicine, 47*, 590–598. https://doi.org/10.1097/RLU.0000000000004146.

[19] Yang, Y., Cheng, J., Peng, Z., Yi, L., Lin, Z., He, A., Jin, M., Cui, C., Liu, Y., Zhong, Q., & Zuo, M. (2023). Development and validation of contrast-enhanced CT-based deep transfer learning and combined clinical-radiomics model to discriminate thymomas and thymic cysts: A multicenter study. *Academic Radiology*. https://doi.org/10.1016/j.acra.2023.10.018.

[20] Chang, C. C., Tang, E. K., Wei, Y.-F., Lin, C. Y., Wu, F. Z., Wu, M. T., Liu, Y.-S., Yen, Y.-T., Ma, M., & Tseng, Y. L. (2023). Clinical radiomics-based machine learning versus three-dimensional convolutional neural network analysis for differentiation of thymic epithelial tumors from other prevascular mediastinal tumors on chest computed tomography scan. *Frontiers in Oncology, 13*. https://doi.org/10.3389/fonc.2023.1105100.

[21] Nakajo, M., Harada Takeda, A., Katsuki, A., Jinguji, M., Ohmura, K., Tani, A., Sato, M., & Yoshida, T. (2022). The efficacy of 18F-FDG-PET-based radiomic and deep-learning features using a machine-learning approach to predict the pathological risk subtypes of thymic epithelial tumors. *British Journal of Radiology, 95*(1134). https://doi.org/10.1259/bjr.20211050.

[22] Onozato, Y., Suzuki, H., Matsumoto, H., Ito, T., Yamamoto, T., Tanaka, K., Sakairi, Y., Matsui, Y., Iwata, T., Iida, T., Iizasa, T., & Yoshino, I. (2023). Machine learning models from computed tomography to diagnose thymic epithelial tumors requiring combined resection. *Journal of Thoracic Disease, 16*, 4935–4946. https://doi.org/10.21037/jtd-23-1840.

[23] Tan, S., Chen, J., Wang, Z.-G., Zhao, X., Sun, Y., Zhu, Y., Gong, Z., & Zhang, D. (2022). Genomic characterization of thymic epithelial tumors reveals critical genes underlying tumorigenesis and poor prognosis. *Clinical Genetics, 103*(5), 529–539. https://doi.org/10.1111/cge.14285.

[24] Zhang, X., Zhang, P., Cong, A., Feng, Y., Chi, H., Xia, Z., & Tang, H. (2023). Unraveling molecular networks in thymic epithelial tumors: Deciphering the unique signatures. *Frontiers in Immunology, 14*. https://doi.org/10.3389/fimmu.2023.1264325.

[25] Li, Z., Wang, F., Zhang, H., Zheng, H., Zhou, X., Wang, Z., Xie, S.-L., Peng, L., Wang, X., & Wang, Y. (2023). The predictive value of a computed tomography-based radiomics model for the surgical separability of thymic epithelial tumors from the superior vena cava and the left innominate vein. *Quantitative Imaging in Medicine and Surgery, 13*, 5622–5640. https://doi.org/10.21037/qims-22-1050.

[26] Zhang, H., Chen, H., Qin, J., Wang, B., Ma, G., Wang, P., Zhong, D., & Liu, J. (2022). MC-ViT: Multi-path cross-scale vision transformer for thymoma histopathology whole slide image typing. *Frontiers in Oncology, 12*. https://doi.org/10.3389/fonc.2022.925903.

[27] Caron, M., Misra, I., Mairal, J., Goyal, P., Bojanowski, P., & Joulin, A. (2020). Unsupervised learning of visual features by contrasting cluster assignments. *Advances in Neural Information Processing Systems, 33*, 9912–9924.

[28] Chen, T., Kornblith, S., Norouzi, M., & Hinton, G. (2020). A simple framework for contrastive learning of visual representations. *Proceedings of the 37th International Conference on Machine Learning*, 119, 1597–1607.

[29] He, K., Fan, H., Wu, Y., Xie, S., & Girshick, R. (2020). Momentum contrast for unsupervised visual representation learning. *Proceedings of the IEEE/CVF Conference on Computer Vision and Pattern Recognition (CVPR 2020)*, 9729–9738. https://doi.org/10.1109/CVPR42600.2020.00975.

[30] Möhrmann, L., Rostock, L., Werner, M., Oleś, M., Arnold, J. S., Paramasivam, N., Jöhrens, K., et al. (2025). Genomic landscape and molecularly informed therapy in thymic carcinoma and other advanced thymic epithelial tumors. *Med*. https://doi.org/10.1016/j.medj.2025.100612.

[31] Grill, J.-B., Strub, F., Altché, F., Tallec, C., Richemond, P. H., Buchatskaya, E., Doersch, C., Pires, B. A., Guo, Z., Azar, M. G., Piot, B., Kavukcuoglu, K., Munos, R., & Valko, M. (2020). Bootstrap your own latent: A new approach to self-supervised learning. *Advances in Neural Information Processing Systems, 33*, 21271–21284.